MAX PLANCK INSTITUTE
FOR SOLAR SYSTEM RESEARCH

# Double Side Photospheric Flux Transport Model Combining Near-side and Far-side Information

Stephan G. Heinemann[1,✉] · Dan Yang[1,✉]

[1]Max Planck Institute for Solar System Research, 37077 Göttingen, Germany
✉ stephan.heinemann@hmail.at; heinemann@mps.mpg.de; yangd@mps.mpg.de

## Introduction

Synoptic magnetic field data usually serves as input for simulations of the global magnetic field; however, it has been shown that these data suffer from an "aging effects" as the longitudinal 360° information can only be obtained over the course of one solar rotation. This can introduce significant uncertainty in subsequent analysis. And it has been shown that there is a large disparity (over a factor of 2) between the open magnetic flux observed by remote sensing and the flux measured in-situ (Linker et al., 2019, 2021, Wang et al., 2022). The source of this discrepancy is not well known; however, the lack of 360° magnetic field information might play a significant role.

Different authors have successfully demonstrated that some magnetic field information can be derived from STEREO/EUVI observations. Heinemann et al. (2021) used 304Å filtergrams to empirically derive the open fields of far-side coronal holes, Kim et al. (2019) and Jeong et al. (2022) used AI and machine learning to produce magnetic field maps from EUV observations. However, this dependence on STEREO observations constrains the information to time periods where the STEREOs observed the solar far side. Arge et al. (2013) tested the inclusion of far-side active region (AR) derived from helioseismic measurements into the ADAPT model and showed that the WSA modeled solar wind values better agree with the in-situ measurements.

Helioseismic imaging is a powerful way to detect the emergence and to track the evolution of individual active regions on the Sun's far side by using observations of the solar 5-min oscillations. Acoustic waves propagate in the solar interior and connect the far side to the Earth side of the Sun. These waves travel faster in magnetized regions, most likely due to the Wilson depression, hence have the potential to detect active regions along their paths of propagation. Lindsey & Braun (2000) evidently proved this concept to work by cross-correlating the forward and backward propagated waves (in time) at target locations on the far side and demonstrated a clear distinction between phase shifts in active regions and in quiet Sun. The method is now known as far-side imaging and is routinely used to monitor the Sun's far side.

Here we propose a new magnetic field data product, that systematically includes newly emerged far-side active regions to provide accurate 360° magnetic field information as input to solar and heliospheric models. We use 720s line-of-sight magnetograms from HMI to accurately represent the magnetic field on the Earth-facing side and insert active regions detected by a state-of-the-art helioseismic measurements (Yang & Gizon in prep.) on the far side into a modified surface flux transport model (SFTM; Baumann, 2005).

## Far-Side Active regions

Synchronic magnetic maps on the Sun's surface computed by using surface flux transport models (see, Jiang et al. 2014, and references therein) are an important boundary condition for space weather modeling. In order for helioseismic far-side images to be applied to these models, the measured phase shifts need to be converted into magnetic fields. This conversion can be done by using an empirical approach, as far-side seismic signals are found to be correlated to magnetic fields (Hernández et al. 2007). Here, we apply state-of-the-art far-side maps, which have the highest active-region detection rate among existing seismic imaging techniques (Yang & Gizon in prep.), to a SFTM. By comparing output synchronic magnetograms from evolving Earth-side SDO/HMI magnetograms with far-side seismic maps, we find a power law between the seismic measurements and the unsigned magnetic fluxes for active regions on the far-side. Specifically, a simple threshold is applied to seismic maps (Fig.1 (a,b)) to determine the locations of active regions. The fluxes within the detected regions are compared to the unsigned flux of the SFTM output magnetograms if active regions are present in both two datasets. Active region magnetic fields are assumed to be symmetric with respect to local minima in the detected seismic regions, and to follow Gaussian distributions with the same widths of the seismic signals. Amplitudes for the Gaussians are determined by the power law for the unsigned fluxes and by forcing the total magnetic flux of the active region to be zero, with the polarity determined by Hale's law and Joy's law (Fig.1 (c)). Currently, we only include bipolar emerging active regions on the far side into the SFTM, but other types of seismic detected regions will be included into our model in the near future.

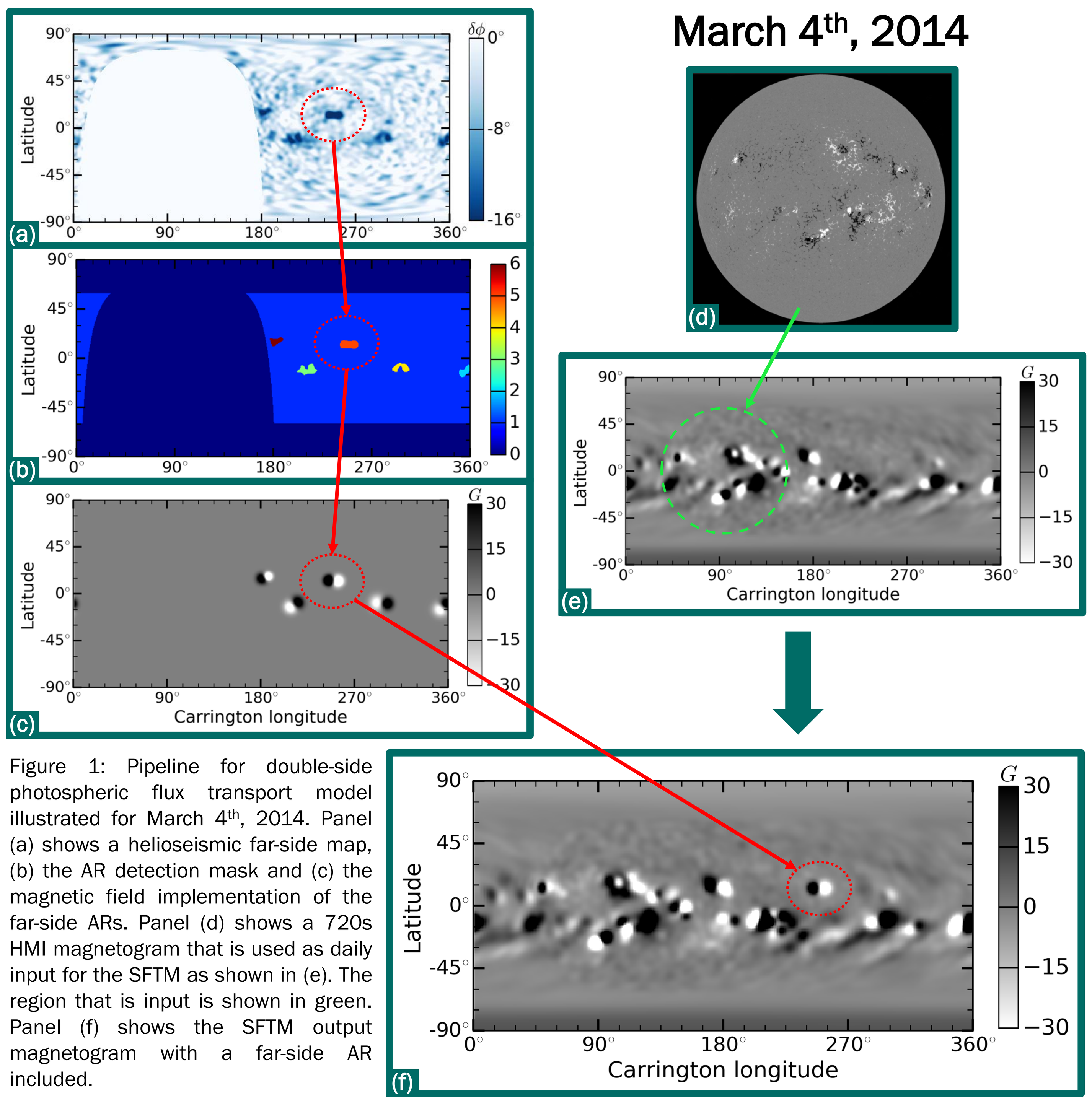


Figure 1: Pipeline for double-side photospheric flux transport model illustrated for March 4th, 2014. Panel (a) shows a helioseismic far-side map, (b) the AR detection mask and (c) the magnetic field implementation of the far-side ARs. Panel (d) shows a 720s HMI magnetogram that is used as daily input for the SFTM as shown in (e). The region that is input is shown in green. Panel (f) shows the SFTM output magnetogram with a far-side AR included.

## Surface Flux Transport Model

We use an adapted Surface Flux Transport Model (SFTM) based on Baumann (2005). With the assumption of radially oriented photospheric field, we use the induction equation to compute the time dependent magnetic field $B_r$ according to:

$$\frac{\partial B_r}{\partial t} = -\omega(\theta)\frac{\partial B_r}{\partial \varphi} - \frac{1}{R_\odot \sin\theta\ \partial\theta}\left(v(\theta)B_r\ \sin\theta\right) + \frac{\eta_h}{R_\odot^2}\left[\frac{1}{\sin\theta}\frac{\partial}{\partial\theta}\left(\sin\theta\frac{\partial B_r}{\partial\theta}\right) + \frac{1}{\sin^2\theta}\frac{\partial^2 B_r}{\partial\varphi^2}\right]$$

with co-latitude $\theta$, longitude $\varphi$, solar radius $R_\odot$, differential rotation $\omega(\theta)$, meriodal flow $v(\theta)$ and the effective diffusion coefficient associated with non-stationary supergranular motions $\eta_h$. Every day, we input the central region of 720s HMI/SDO line-of-sight magnetograms with $|\theta| \leq 60°$ and $|\varphi| \leq 60°$ (see Fig.1 (d,e)), thus keeping the near-side up to date. The magnetic field that is out of Earth's field-of-view evolves according to our SFTM; however, it is known that new ARs can emerge on the solar far side. This has the implication that the any magnetogram spanning 360° in longitude shows an outdated and wrong magnetic field structure until the newly emerged region has rotated to the front side. To provide an accurate representation of the far-side magnetic field, we input newly emerged ARs that have been detected and extracted by advanced far-side helioseismology.

## Potential Field Extrapolations

To compare magnetograms with and without inserted far-side ARs, we perform potential field extrapolations (PFSS; Altschuler & Newkirk, 1969; Schatten et al., 1969) using a python implemented finite-difference scheme (pfsspy; Stansby et al., 2020). In Figure 2, we show the PFSS results for March 4th, 2014 using a source surface radius of $R_{SS}$=2.3. The overplotted field lines show that a significant reconfiguration of the local magnetic field structure occurs when inserting an far-side AR (Fig. 2, top panels). We also find global implications: the heliospheric current sheet (Fig. 2, middle panels) as shown in the source surface magnetic field clearly shifts position and the area of the coronal hole (i.e., open fields) located to the south of the inserted AR changes (Fig. 2, bottom panels). The inserted field reconfigures not only the surrounding (especially closed) field but may also reconnect with distant (e.g., $\Delta\theta > 50°$) structures causing global changes in the open field structure. The differences are shown in Figure 2 (c).

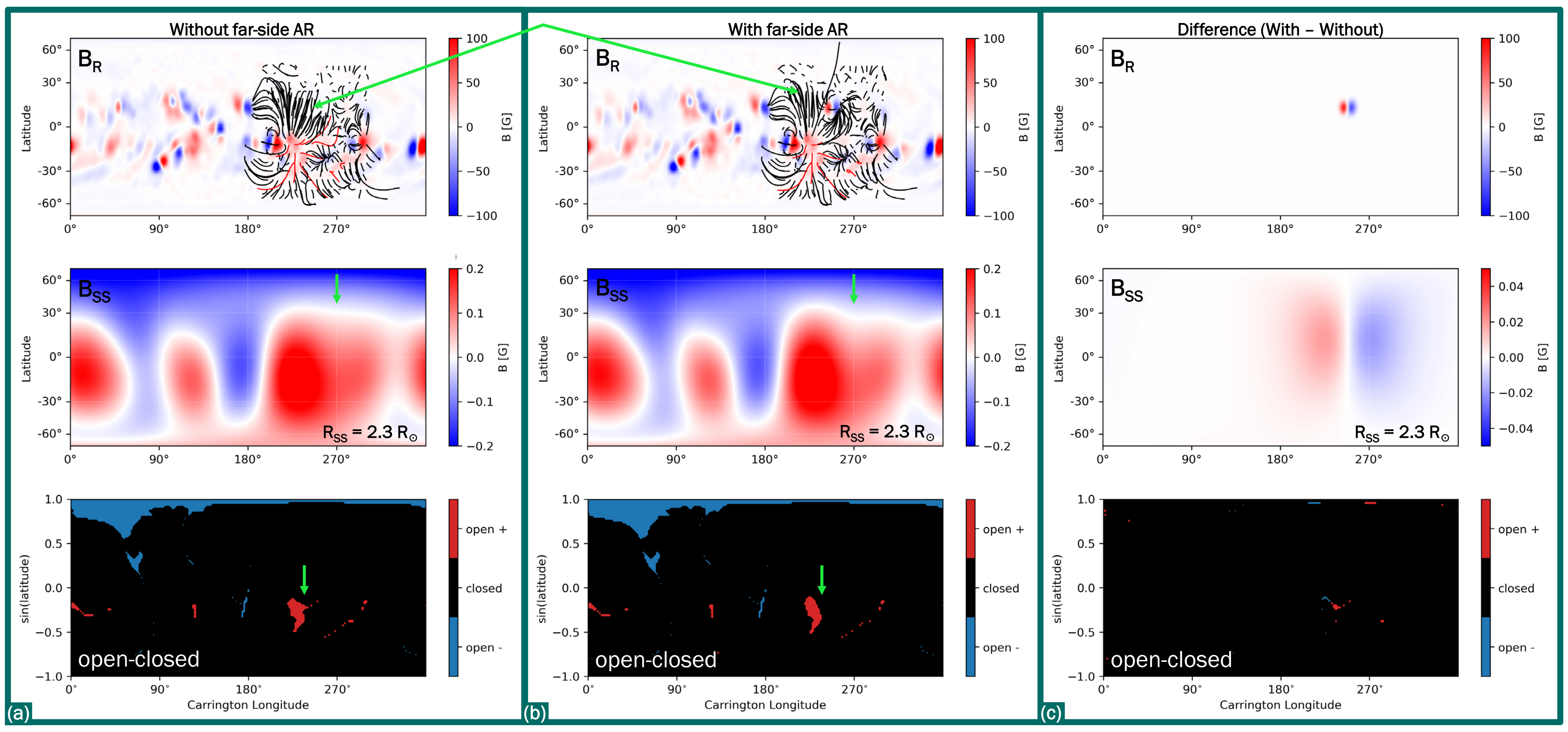


Figure 2: PFSS extrapolation from the SFTM generated magnetograms on March 4th, 2014. Panel (a) shows the results for the magnetograms without inserted far side AR, (b) shows the results with the inserted newly emerged AR and (c) shows the difference between (b) and (a). The top panels show the photospheric magnetic field with overplotted field lines (for (a) and (b) only, closed field lines in black and open field lines in red/blue) in a region surrounding the inserted AR. The middle panels show the source surface magnetic field at a source surface radius of 2.3 $R_\odot$ and the bottom panel shows the traced open fields at 1.01 $R_\odot$. The green arrows mark major differences between the results with and without inserted far-side AR.

## Summary & Outlook

We generate a new magnetic field data product using a modified SFTM with input from near-side HMI/SDO magnetograms and far-side active regions detected by improved helioseismic holography based on HMI/SDO dopplergrams. We find that inserted ARs significantly reconfigure the local magnetic field and can also change the global magnetic field structure. This may lead to changes in the modeled and forecast solar wind properties in interplanetary space. We evaluated PFSS results of our SFTM magnetograms against those of ADAPT magnetograms (Arge et al., 2010, Hickmann et al., 2015) and find very similar results using the same spatial resolution and the maps without the inserted ARs. Differences can be found when using the maps with the inserted far-side ARs.

*Further steps:*

- Currently, far-side regions are modeled as bi-polar regions with two poles of comparable strength. ARs mainly consisting of 1 or 3 poles are neglected. We are currently working on extracting the AR configuration from helioseismic images and the according implementation into the SFTM.
- We use helioseismic holography to detect all ARs of a certain size and strength, but only newly emerged ARs are inserted into the SFTM. We are exploring the option in correcting existing far-side regions in the SFTM using their representation derived from helioseismology.
- Thorough testing and evaluation, especially in the heliospheric domain (e.g., solar wind, space weather forecast, interplanetary magnetic field structure) will be done in the future.
- Although we use state-of-the-art values for differential rotation and meriodal flows, there are still parameters (e.g., diffusion coefficient) that need to be tuned.

## References

- Altschuler, M. D., & Newkirk, G. 1969, SoPh, 9, 131
- Arge, C. N., et al. 2013, AIPC Vol.1539, 11–14
- Arge, C. N., et al. 2010, AIPC, Vol. 1216, 343–346
- Baumann, I. J. 2005, PhD thesis,
- González Hernández C., et al. 2007, ApJ, 669, 1382
- Heinemann, S. G., et al. 2021, SoPh, 296, 141
- Hickmann, K. S., et al. 2015, SoPh, 290, 1105
- Jeong, H.-J., et al. 2022, arXiv, arxiv.org/abs/2204.12068
- Jiang, J., et al. 2014, SSRv, 186, 491
- Kim, T., et al. 2019, Nature Astronomy, 3, 397
- Lindsey, C., et al. 2000, Science, 287, 1799
- Linker, J. A., et al. 2017, ApJ, 848, 70
- Linker, J. A., et al. 2021, ApJ, 918, 21
- Schatten, K. H., et al. 1969, SoPh, 6, 442
- Stansby, D., et al. 2020, JOSS, 5, 2732
- Wang, Y. M., et al., 2022, ApJ, 926, 113

## Acknowledgements

Both authors contributed equally to this project. The SDO image data is available by courtesy of NASA and the respective science teams. S.G.H. and D.Y. thank L.G. for funding and supporting this study.